UNIVERSITY OF AMSTERDAM

UvA-DARE (Digital Academic Repository)

A molecular perspective on the cleaning of oil paintings

Baij, C.L.M.

[Link to publication](#)

TIME-DEPENDENT ATR-FTIR SPECTROSCOPIC STUDIES ON SOLVENT DIFFUSION AND FILM SWELLING IN OIL PAINT MODEL SYSTEMS

2.1 Introduction

Paintings are exposed to organic solvents or aqueous solutions during restoration or cleaning procedures. These cleaning actions may induce many types of undesirable chemical changes,[28–31] which are often not immediately visible to the restorer. At present, our understanding of the influence of solvent treatment on fundamental chemical processes is too limited to make a reliable estimate of the long-term effects of common restoration procedures. For example, it is unclear to which depth solvents typically penetrate during cleaning and to what degree soluble components are transported between paint layers. Although the rate of transport processes of soluble components can vary considerably between paintings and cleaning methods,[32] the degree of paint swelling and the rate of solvent diffusion are both important factors.

The binding medium in oil paint consists of triacylglycerides (TAGs) that have a high degree of unsaturation on their fatty acid chains. As it dries through autoxidation, the oil forms a strongly cross-linked polymer network.[4–6,33–41] The presence of potentially reactive metal-containing pigments and a variety of additives further adds to the complexity of aged oil paint. Oil paint can be considered metastable polymers, subject to slow chemical and physical deterioration processes that affect the appearance and structural integrity of oil paintings.

We have previously demonstrated that mixtures of oil binding media and ZnO or PbO gradually form an *ionomer*-like structure.[42,43] In such an ionomer structure, metal ions originating from pigments or driers are distributed throughout the polymerised oil network and associated to carboxylic acid groups. Ionomer-like structure has been detected in many oil paint layers that contain lead or zinc ions. We have developed ionomer model systems for aged oil paint to study the molecular structure and dynamic processes in paintings. These models consist of linseed oil polymerised with lead or zinc sorbate (2,4-hexanedieneoate) complexes, as illustrated in Scheme 2.1. In previous work, small angle X-ray scattering (SAXS) measurements on these ionomer systems indicated that metal carboxylates form clusters in oil polymers,[43] and we showed that the reaction of saturated fatty acids with network-bound metal carboxylates is a rapid process that is accelerated by solvent swelling.[29] In this study of solvent behaviour, we have employed the same model systems for aged oil paint (**Pbpol** and **Znpol**), and included films of pure polymerised linseed oil (**pLO**) and films pigmented with ZnO (**ZnO-LO**) for comparison. The pigmented system has the same ionomeric structure in the polymer binding medium as **Znpol**,[43] so differs from the pure ionomer system only in the presence of ZnO pigment particles. We also study the kinetics of solvent delivery of three cleaning gels on our model systems for aged oil paint binding medium.

When investigating the solvent diffusion and swelling behaviour of a polymer, it is important to know if the system is studied above or below the glass transition temperature (T_g). It is well known that the T_g of polymers can strongly influence solvent diffusion
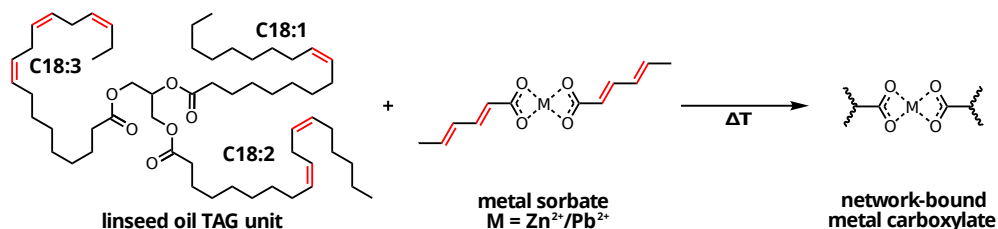
Scheme 2.1 The formation of ionomers by co-polymerisation of linseed oil with metal sorbate. Linseed oil is represented by a typical structure of a triacyl glycerol (TAG) unit. The depicted carboxylate coordination geometry does not reflect the real geometry (see Chapter 5).

behaviour. Above the T_g (in the rubbery region), polymers generally show Fickian (ideal) sorption, whereas polymers can show strong deviations from ideal behaviour below their T_g (glassy regime).[44] Therefore, we have studied the viscoelastic properties of our model systems and used dynamic mechanical analysis (DMA) to determine their T_g.

Time-dependent attenuated total reflection Fourier transform infrared (ATR-FTIR) spectroscopy was used to follow swelling and diffusion processes in our ionomeric model systems.[45] This approach has been applied before to study single or multicomponent solvent diffusion,[46–48] solute diffusion from an external medium into a polymer,[49,50] polymer chain inter-diffusion[51,52] and metal ion diffusion in ionomers.[51] Diffusion and swelling by organic solvents[53–56] and water[57–61] in polymer blends based on linseed oil has been measured before using a variety of methods. For ionomers, data on diffusion and swelling is mainly limited to water and alcohols for fuel cell applications.[62–66] In most of these studies, polymer films are cast from solution (*e.g.* by spin-coating or dip-coating) directly onto the ATR elements as thin films to ensure a good contact. However, polymer films based on drying oils are insoluble due to their high degree of cross-linking and our model systems did not adhere well to ATR elements. To meet the challenge of maintaining a reproducible and constant contact between polymerised oil films and the ATR crystal during solvent swelling, we developed a measurement setup that can be combined with a standard diamond ATR module in which a very small constant pressure is applied on the sample during solvent exposure. The method allows the measurement of dynamic processes in unsupported film-like materials with at least one smooth surface (*e.g.* paints, polymers, gels or skin). Finally, to fully describe the process of solvent sorption in oil-based polymers, we have developed a combined diffusion/swelling model based on a polymer fraction dependent diffusion coefficient.

Combining new insights on the viscoelastic properties of oil paint model systems and the swelling and diffusion behaviour of water and other solvents, this work aims to provide a better understanding of solvent action on oil paints to support the development of improved conservation and restoration strategies.

2.2 Results and discussion

2.2.1 DMA analysis of model paint films

The viscoelastic properties of the model ionomer and paint systems were characterised by DMA. Figure 2.1 and Table 2.1 present glass transition temperature and cross-link density data for ionomer films with increasing metal content (from 0% neutralisation to 100%), as well as pure polymerised linseed oil (**pLO**) and ZnO-based paint (**ZnO-LO**). The T_g values were obtained from the maximum of the tan δ plots (note that tan $\delta = E''/E'$, where E'' and E' are the loss and storage modulus values, respectively).

At present, there is some uncertainty in the literature on the T_g of linseed oil-based paint films. Previous studies reported values between 0 and 10 °C,[67–70] while Ploeger *et al.*[71] observed an increase to around 40 °C upon aging of the paint films. LO polymers modified with styrene[72] or epoxy groups[73] tend to have a higher T_g. We found a T_g for **pLO** at 8 °C. The T_g is raised slightly to 10 °C upon co-polymerisation with sorbic acid (**Mpol-0**, essentially an 'empty' ionomer), suggesting possible hydrogen bonding between adjacent acid groups.[74]

For the lead ionomers (**Pbpol**), the characteristic behaviour of a two phase system was observed. It is known that, in a relatively apolar polymer matrix, the introduction of ionic groups can lead to the formation of ionic aggregates,[75,76], giving rise to ion-poor (*i.e.* polymer matrix) and ion-rich (*i.e.* metal carboxylate cluster region) phases. The tan δ peak at low temperature is attributed to the bulk T_g, while the peak at higher temperatures corresponds to the glass transition in the ion-rich regions (T_c). This T_c peak grows at the expense of the main glass transition peak and shifts to higher temperatures as the ion content increases. In contrast to T_c, the 'matrix' T_g for **Pbpol** shifts to lower temperatures when the ion-content is increased. The shifts in T_g and T_c suggest that there are changes in the structure or composition of the ion-poor and ion-rich phases in **Pbpol** with increasing lead content, not just in the concentration of ion-rich clusters. In previous research, SAXS analysis on **Pbpol** samples showed that long-range inhomogeneity in lead concentration exist at low neutralisation levels, while lead ions tended to be grouped in smaller and more defined ion-rich clusters at high neutralisation.[43] In line with these observations, to explain the trends in T_g and T_c we propose that the lead carboxylate concentration (and therefore also the cross-link density) decreases in the bulk polymer with increasing neutralisation leading to lower T_g values, while at the same time the ion-rich phases become more enriched in lead, leading to a rise in T_c.

Considering **Znpol**, it was observed that increasing the zinc content has no significant effect on the T_g values. No T_c was observed for **Znpol** in the measured temperature range, though Figure 2.1b seems to suggest there could be a transition (> 150 °C) that is related to ion cluster relaxation. A very high T_c would be in agreement with the fact that the formation of crystalline zinc soaps in ionomeric polymer systems is much slower than the
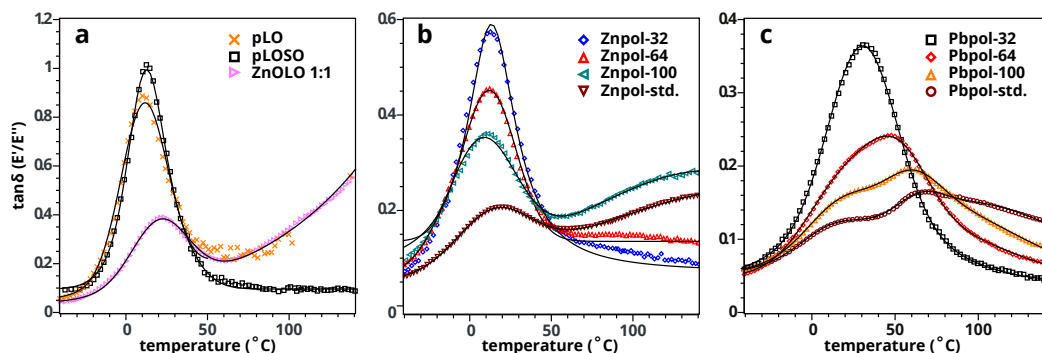
Figure 2.1 DMA thermograms showing **a Mpol-0**, **pLO**, **ZnO-LO** and **b Znpol** and **c Pbpol** ionomer systems with increasing metal content.

Table 2.1 T_g, T_c and ν_e values for **pLO**, **ZnO-LO**, **Mpol-0**, **Znpol** and **Pbpol** ionomer systems with increasing metal content. COOM/COOH refers to the proportion of sorbic acid groups that is coordinated to a metal ion (Zn^{2+} or Pb^{2+}).

Sample	$\frac{COOM}{COOH}$	T_g (°C)	T_c (°C)	ν_e (mol/cm^3)
pLO	0	8	–	2.1×10^{-5}
Mpol-0	0	10	–	3.5×10^{-4}
Pbpol-32	0.32	33	31	8.5×10^{-4}
Pbpol-64	0.64	20	53	1.2×10^{-3}
Pbpol-100	1	17	61	4.0×10^{-3}
Pbpol-std.	1	11	67	4.8×10^{-3}
Znpol-32	0.32	11	–	6.3×10^{-4}
Znpol-64	0.64	10	–	6.8×10^{-4}
Znpol-100	1	9	–	8.6×10^{-4}
Znpol-std.	1	16	–	2.2×10^{-3}
ZnO-LO	–	21	–	5.6×10^{-4}

formation of lead soaps.[29,77] The tan δ peaks close to room temperature decreased strongly in height with increasing zinc content, which is thought to reflect a decreasing mobility of the polymer chain segments.[78] While decreasing chain mobility seems plausible with increasing zinc carboxylate content, SAXS measurements on **Znpol** systems showed no clear trend in either the concentration or the size of ionic domains with increasing zinc neutralisation.[43] Clearly, more DMA and SAXS experiments on systems with a wide neutralisation range are necessary to clarify the structural details of linseed oil-based ionomers.

The T_g of **ZnO-LO** was measured at 21 °C. The slightly higher T_g for **ZnO-LO** might be explained by the lower degree of curing for **ZnO-LO** (1 week at 60 °C) compared to **Znpol** (17 h at 150 °C). In previous studies, Phenix[69] could only detect 'progressive, general
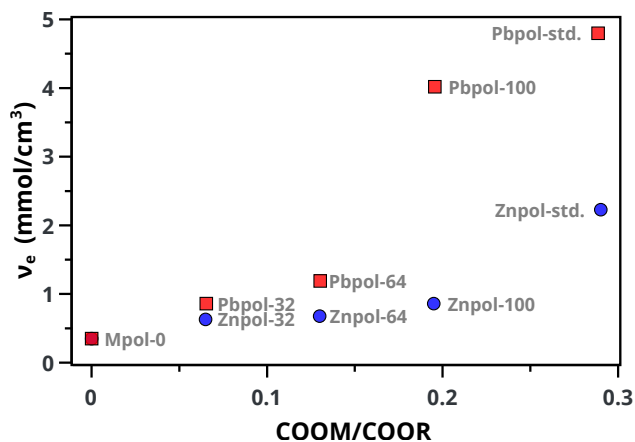
Figure 2.2 The relation between ion content and ν_e as calculated by Eq. 2.1.

thermal softening' in 16 year old ZnO paint, possibly due to a higher pigmentation.

The elasticity modulus E' in rubbery plateau region at 140 °C (see Figure B.3) was used to calculate cross-link densities (ν_e) according to[79]

$$\nu_e = \frac{E'}{3RT} \tag{2.1}$$

The calculated values for ν_e as a function of metal carboxylate concentration (COOM/COOR) are shown in Figure 2.2. Both for **Znpol** and **Pbpol**, ν_e increases significantly with metal content. Ionic cross-links thus contribute significantly to the measured storage modulus and calculated cross-link densities, despite the fact that the unbound carboxylic acids in the not fully neutralised ionomers can also form 'cross-links' by hydrogen bonding. In analogy with Weiss *et al.*,[80] we also calculated a cross-link density by assuming that every metal sorbate unit forms an additional cross-link (ν_c) on top of the cross-link density of **Mpol-0**, and compared this with ν_e calculated from Eq. 2.1. It was found that ν_e was consistently higher than ν_c by approximately 5–20%. In the paper by Weiss *et al.*,[80] two possible explanations are given for this high contribution of metal neutralisation to ν_e:

1. Synergism exists between the ionic cross-links and molecular entanglements that yield a higher effective cross-link density than that based on a linear combination of the two effects;

2. ionic clusters have a lower molar mass between cross-links than that calculated from the average chain length between simple contact ion-pair associations.

Since we are currently primarily concerned with solvent behaviour in these oil-based ionomers, the in-depth investigation of these hypotheses is beyond the scope of this work.

Concluding, we established that our model systems have bulk T_g values close to room

temperature. Therefore, (near) Fickian solvent diffusion is expected. The effect of the T_c on solvent diffusion remains to be investigated.

2.2.2 Solvent diffusion and swelling in model paint films

The diffusion and swelling behaviour of seven solvents was investigated in **Znpol**, **Pbpol** and **ZnO-LO** model systems. Solvent concentration profiles were obtained by integration of characteristic solvent IR bands. The maximum swelling capacity of each solvent was determined by monitoring the IR absorption bands corresponding to the linseed oil polymer. As solvent diffused into the volume probed by the IR beam, the concentration of polymer chains in that volume decreased according to a profile that mirrored the solvent diffusion profiles. Since it was shown previously[81] that FTIR spectroscopy can be used to measure swelling factors that are equivalent to those obtained from size measurements using a CCD camera, the relative difference in absorption of the ester carbonyl band (1740 cm^{-1}) at saturation and at $t = 0$ (*i.e.* $\Delta A / A_0$) was used as a measure for the maximum degree of swelling (f_{eq}). Values for f_{eq} for all solvents and samples are given in Table 2.3.

A significant variation in the solvent swelling capacity was observed. DCM swelled the investigated model systems by more than a factor of 2, while water hardly swells the oil polymer at all (approximately 5 to 10 % volume increase for zinc and lead, respectively). The FTIR spectroscopic method for measuring equilibrium swelling accurately reproduces trends reported in the literature for solvent swelling of oil paints, and confirms the low swelling capacity of water.[82,83] The trends in f_{eq} for different solvents are consistent between all three investigated polymers. It is noted that for low-swelling solvents such a cyclohexane and water, the differences between **Znpol** and **Pbpol** are larger. In the case of cyclohexane in **Pbpol**, it was not possible to carry out the diffusion experiment at room temperature due to detachment of the rather stiff polymer film from the ATR crystal during solvent exposure. Therefore, this measurement was conducted at 40 °C. Despite the differences in viscoelastic properties that were measured with DMA, no significant differences in f_{eq} between **Znpol** and **Pbpol** were found (standard deviation in f_{eq} of $\pm$ 0.13, see Experimental section). However, **ZnO-LO** *did* exhibit consistently lower values for f_{eq} than the unpigmented ionomer films. This result is explained by the fact that the pigment particles do not contribute to the swelling of the system upon solvent absorption.

2.2.3 The Fickian diffusion model

Diffusion in films exposed to liquid solvent

A Fickian diffusion model for ATR-FTIR has been developed by Fieldson and Barbari[45], which allows for the calculation of diffusion parameters using the recorded IR spectra. Having established that the model systems under investigation have T_g values close to room temperature, we investigated the applicability of this Fickian diffusion model. A

typical concentration profile for acetone, toluene-d_8 and methanol-d_4 in **Znpol** is shown in Figure 2.3. For ideal diffusion with a constant diffusion coefficient, Fick's second law states

$$\frac{\partial C}{\partial t} = D \left(\frac{\partial^2 C}{\partial x^2} \right) \tag{2.2}$$

where C is the concentration of penetrant in the medium, and D is the diffusion coefficient. A solution to this differential equation has been derived by Fieldson and Barbari[45] using appropriate boundary conditions for the geometry of an ATR-FTIR setup, making use of the exponential decay of the evanescent field of the IR beam into the sample and the Beer-Lambert law

$$\frac{A(t)}{A(\infty)} = 1 - \frac{8\gamma}{\pi(1 - \exp[-2\gamma\delta])}$$
$$\sum_{n=0}^{\infty} \left[\frac{\exp[-Df^2t] \left(f \exp[-2\gamma\delta] + 2\gamma(-1)^n \right)}{(2n+1)(4\gamma^2 + f^2)} \right] \tag{2.3}$$

in which

$$f = \frac{(2n+1)\pi}{2\delta}$$

and

$$\gamma = \frac{2n_2\pi}{\lambda} \sqrt{\sin^2\theta - \left(\frac{n_1}{n_2} \right)^2} \tag{2.4}$$

In this relation, γ is the inverse of the penetration depth d_p of the IR beam into the sample. d_p varies from 0.5 to 3.5 μm from 3500 to 500 cm^{-1} in our experiments, so with a typical film thickness around 150 μm the recorded spectra are representative for the bottom side of the film. Parameters n_1 and n_2 are the refractive indices of the polymer sample and ATR crystal, respectively, δ is the thickness of the film, θ is the angle of incidence of the IR beam (45°), and λ is the wavelength corresponding to the maximum of the characteristic IR band of the penetrant. For the experimental conditions described in this chapter, the shape of the diffusion profile is very insensitive to the exact value of γ. Therefore, a single measured value for the refractive index of a **Znpol** film was assumed as a constant for all calculations. This model represents an ideal case of penetrant transport (*i.e.* negligible preferential interaction between the polymer and solvent), corresponding to a diffusion of penetrant that is on a much slower timescale than polymer chain relaxation.[44]

Fitting Eq. 2.3 to the diffusion curve of acetone, toluene-d_8 and methanol-d_4 in **Znpol**, it is immediately clear that the ideal model is not capable of described simultaneously the long delay until solvent signal is first detected as well as the sharp increase in solvent concentration that follows (see Figure 2.3, blue curves). Similar results were found for all investigated solvents and films. While Eq. 2.3 is frequently applied to describe penetrant
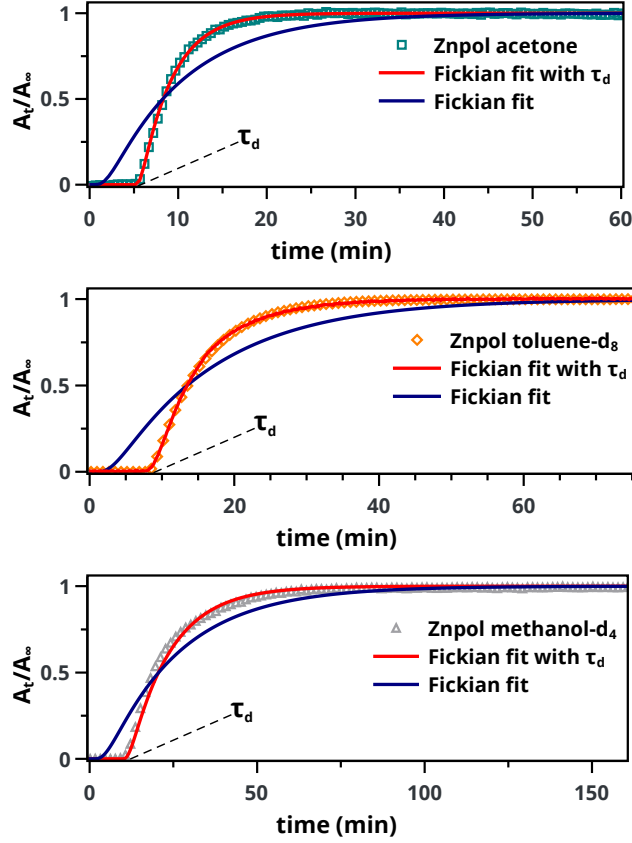
Figure 2.3 Concentration profile for acetone, toluene-d_8 and methanol-d_4 in **Znpol** using a standard (blue) and adapted (red) Fickian diffusion model to fit the data. The standard Fickian model clearly does not predict the delay time τ_d.

diffusion in polymers, our use of relatively thick films enhances the effect of potential polymer swelling during diffusion, and it causes a significant delay time (τ_d, the time necessary for solvent to reach the sampling volume). Therefore, using thick polymer films, it becomes easier to investigate deviations from ideal diffusion behaviour.

To allow for the considerable delay time, τ_d, Eq. 2.3 was adapted such that

$$\frac{A(t)}{A(\infty)} = \begin{cases} 0 \,, & \text{for} \quad 0 < t < \tau_d \\ \frac{A(t-\tau_d)}{A(\infty)} \,, & \text{for} \quad t \geq \tau_d \end{cases} \tag{2.5}$$

With this procedure, the swelling between $0 < t < \tau_d$ is neglected, while Fickian diffusion is assumed at $t > \tau_d$. The shifted Fickian model of Eq. 2.5 provided a near-perfect fit to the experimental concentration profiles, as shown in Figure 2.3. Corresponding diffusion coefficients D_{Fick} are listed in Table 2.3.

From the excellent match between the ideal diffusion model and the experimental concentration profiles at $t > \tau_d$, it can be concluded that once the polymer is nearly completely swollen (*i.e.* only minor changes in polymer fraction), (near) Fickian diffusion behaviour is observed in the measurement volume at the bottom of the film. However, film swelling *does* cause an significant increase in τ_d. This effect is easily observed by comparing the experimental τ_d values with values calculated with the common relation between δ (thickness) and D, $\delta = \sqrt{D\tau_d}$. The relation yields consistently lower τ_d values than observed experimentally, demonstrating that the ideal diffusion model needs to be replaced by a diffusion model that accounts for film swelling.

In paintings restoration, the swelling of paintings is an important phenomenon. It is well-known that aged oil paint can swell significantly during cleaning and varnish removal.[84] Especially with the relatively short solvent application times typical for restoration work, one might argue that equilibrium swelling (f_{eq}) is never reached, except in the areas of the paint closest to the surface. The initial stages of solvent diffusion are therefore especially relevant to understand the potential effects of restoration treatments on paintings, adding to the importance of developing a model that describes the entire swelling and diffusion process.

Diffusion of solvents released by gels

The shifted Fickian model of Eq. 2.5 was applied to study ethanol and water (D_2O) diffusion released by several cleaning gels.[32] These gels can be used for surface cleaning or varnish removal. The experimental setup is shown in Figure 2.9b. Although the shifted Fickian model does not describes the entire swelling and diffusion process, it allows an accurate estimation of τ and D. In this series of experiments, we measure the diffusion and delay time occurring when a film is exposed to a gel loaded with solvent (Figure 2.9a) and compare the results to those obtained from films exposed to free liquid solvent (Figure 2.9b).

Figure 2.4a shows the concentration profiles of ethanol in the binding medium model for free ethanol, Nanorestore Max Dry gels and 4 % agar gels loaded with ethanol. The difference of the parameter τ between free solvent and solvent released from gels is used as a measure of solvent retention by gels. From Table 2.2, it is evident that the gelled systems do not show significant retention (for **Znpol**: $L^2/\tau = 15 \pm 4$ for free ethanol and $L^2/\tau \simeq 10$ for gelled systems and for **Pbpol**: $L^2/\tau = 7.6 \pm 2.1$ for free ethanol, $L^2/\tau \simeq 8$ for gelled systems). In general, the diffusion coefficient of solvents released from gels in the swollen polymer (at $t > \tau$) is similar (*i.e.* within the experimental error) to the diffusion of free solvents. For example for **Znpol**, free ethanol diffusion has a value of $D = 5.6 \pm 1.8 \times 10^{-8}$ cm^2/s and ethanol released from gels has a value of $D = 7.6 \pm 0.5 \times 10^{-8}$ cm^2/s and $D = 6.6 \pm 2.4 \times 10^{-8}$ cm^2/s, for Nanorestore and agar 4 %, respectively. Likewise, similar diffusion coefficients for free ethanol and ethanol
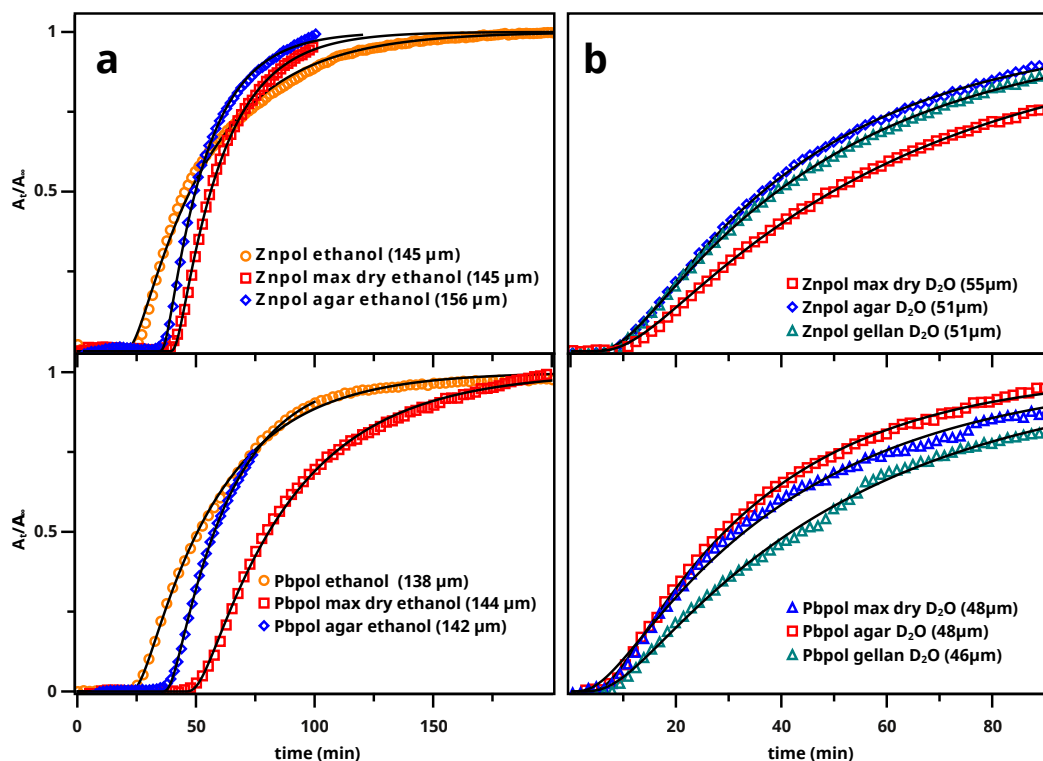
Figure 2.4 Concentration profiles of **a** ethanol and **b** D_2O in zinc and lead ionomer films. Solid black lines represent best fits of the Fickian diffusion model (Eq. 2.5) with a lag time τ as extra parameter. For D_2O, τ was estimated. Only a fraction of all collected data points are shown for clarity.

released from gels were found for **Pbpol**: $D = 3.2 \pm 0.6 \times 10^{-8}$ cm^2/s for free ethanol, $D = 3.40 \pm 0.06 \times 10^{-8}$ cm^2/s for Nanorestore and $D = 5.4 \pm 0.3 \times 10^{-8}$ cm^2/s for agar 4 %. It should be noted that for the gels, evaporation of ethanol from the gel causes loss of contact between the sample and the detector (after $\pm$ 100 min for **Znpol** and $\pm$ 60 min for **Pbpol** with agar) and complete solvent saturation is not reached. The contact loss between sample and ATR crystal did not allow us to quantitatively determine the *amount* of solvent (*e.g.* expressed as swelling) delivered by the gels. Qualitatively though, the solvent delivery from gels appeared to be on par with the application of pure solvents at long timescales.

It was observed that the gels accumulate water on their outer surface, which causes reproducibility issues when the gels are not properly dried before application. When undried, the surface-adhered water seems to be forced into the polymer upon application of the gel. Consequently, τ was close to zero and D up to three times faster for undried gels as compared to surface-dried gels (data not shown). Even when the gels were properly dried, this effect was hard to control. To correct for the error introduced by

Table 2.2 Diffusion coefficients D and lag times corrected for thickness L^2/τ resulting from a fit of the adapted Fickian model to the concentration profiles. Values are averaged over at least two measurements, standard deviations are indicated with $\pm$.

Sample	Solvent	D $(10^{-8}$ cm^2/s$)$	L^2/τ $(10^{-8}$ cm^2/s$)$
Znpol	ethanol	5.1$\pm$1.8	15.0 $\pm$4.0
Znpol + Max Dry	ethanol	7.6$\pm$0.5	9.7$\pm$0.6
Znpol + agar 4%	ethanol	6.6$\pm$2.4	12.0 $\pm$0.3
Znpol	D_2O	0.56$\pm$0.08	8.4$\pm$0.3
Znpol + Max Dry	D_2O	0.39$\pm$0.06	5.4$\pm$0.7
Znpol + agar 4%	D_2O	0.44$\pm$0.07	6.2$\pm$0.2
Znpol + gellan 3%	D_2O	0.39$\pm$0.06	6.5$\pm$0.4
Pbpol	ethanol	3.2$\pm$0.6	7.6$\pm$2.1
Pbpol + Max Dry	ethanol	3.4$\pm$0.06	8.1$\pm$0.0
Pbpol + agar 4%	ethanol	5.4$\pm$0.3	9.1$\pm$1.0
Pbpol	D_2O	0.58$\pm$0.06	7.0$\pm$0.5
Pbpol + Max Dry	D_2O	0.42$\pm$0.14	6.8$\pm$0.3
Pbpol + agar 4%	D_2O	0.42$\pm$0.13	6.4$\pm$1.4
Pbpol + gellan 3%	D_2O	0.32$\pm$0.01	6.7$\pm$0.9

improper drying of the gels, all measurements were performed in duplicate or triplicate. Considering the values of D_{D_2O} for all measurements, some gels (gellan and Max Dry for **Znpol**) show a small but significant decrease in D compared to free water (Table 2.2). We have no mechanistic explanation for this small decrease in D and it is at present unclear if our dataset is large enough to make a solid statistical argument in favour of this minor difference. Comparing the retention (τ) of free water and water released by gels in Table 2.2, no significant increase in τ was found when water was loaded into gels for **Pbpol**, while for **Znpol** there seems to be very limited retention (L^2/τ for **Znpol** is $\simeq 8 \times 10^{-8}$ cm^2/s for free water and $L^2/\tau \simeq 6.5 \times 10^{-8}$ cm^2/s for gels). Clear confirmation of this effect would require a larger data set.

The fact that there is minimal or no effect on τ when water or ethanol is loaded into gels suggests that diffusion is rather determined by the nature (*e.g.* porosity) of the paint surface than by the method of solvent application (free solvent or gels). In order to inhibit solvent retention from the gels, the diffusion of solvent into the paint must be slower than the diffusion of solvent out of the gel. In that case, small amounts of solvent accumulate on the interface of the gel and the surface. This is a key observation for cleaning with gels: it is the paint surface that largely determines the rate of solvent uptake. This argument holds only for non-porous paints, powdery or cracked paints are expected to show faster diffusion by capillary action. Preliminary experiments on a 40 year old porous paint sample confirmed this fast diffusion but posed new analytical challenges that will be the topic of forthcoming research.

2.2.4   The diffusion-swelling model

Construction of the diffusion-swelling model

In the model paint systems, sample swelling to more than twice the original dry volume occurred in the most extreme cases, corresponding to a polymer fraction decreasing from 1 to 0.5. Solvent swelling and diffusion in polymers is widely discussed in the literature.[85–89] The most comprehensive models are those based on the free-volume theory originally developed by Vrentas and Duda.[90,91] However, free-volume models contain many parameters that, despite having physical meaning, are largely unknown. Therefore, we decided to employ the simplest model that accounts for a decreasing polymer volume fraction during swelling, using a variable diffusion coefficient. The functional form of this model is inspired on Cukiers formula for diffusion in hydrogels,[87] and describes a diffusion coefficient that is an exponential function of the polymer volume fraction ϕ as

$$D = D_0 e^{\alpha \phi^\beta} \tag{2.6}$$

Since $D = D_0$ at $\phi = 0$ (pure solvent), for hydrogels D_0 has been interpreted as the diffusion coefficient of solvent molecules in their own environment[88] or at infinite dilution.[87] However, for systems swelling much less than hydrogels, the pre-exponential factor D_0 should be considered as a fitting parameter. Parameter α has been correlated to the radius of solvent molecules.[87] For parameter β, values of 0.5 and 0.75 are mentioned by Amsden.[87] Given the limited range in polymer fraction ϕ for our samples, it was expected that one parameter describing it's effect of diffusion would be sufficient and we assumed $\beta = 1$, yielding a diffusion coefficient dependent only on D_0 and α. As the diffusion coefficient at equilibrium swelling, D_{eq}, is most relevant in the present case, Eq. 2.6 is rewritten as

$$D = D_{eq} e^{\alpha (\phi - \phi_{eq})} \tag{2.7}$$

Here, ϕ_{eq} is the polymer fraction at equilibrium (complete) swelling f_{eq}. Next, the swelling factor F is defined as

$$F = 1/\phi = v_{tot}/v_p = (v_s + v_p)/v_p \tag{2.8}$$

Here, v_s is volume of solvent, v_p is volume of polymer, and v_{tot} is the total volume. The total polymer mass is assumed to occupy the same (partial) volume, v_p, during swelling, while v_s and v_{tot}, do increase. If c_s is the molar solvent concentration, then v_{tot} contains $v_{tot} c_s$ mol solvent of volume v_s. Given the solvent density ρ_s and the solvent molar mass M_s, we know that v_s contains $v_s \rho_s / M_s$ mol of solvent. Therefore

$$v_{tot} c_s = v_s \rho_s / M_s \tag{2.9}$$

Combining Eqs. 2.8 and 2.9 gives the relation between swelling factor and molar solvent
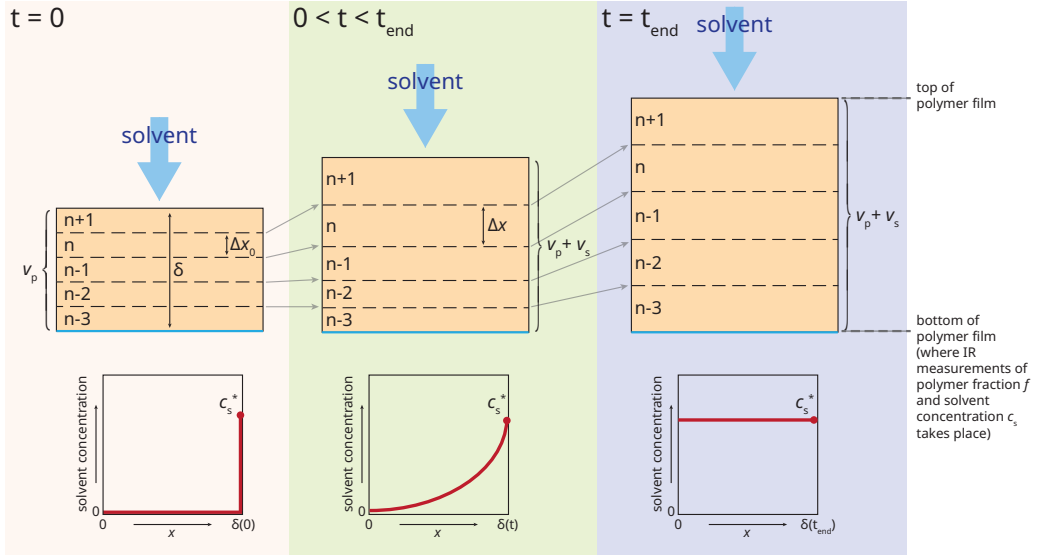
Figure 2.5 Illustration of the method-of-lines model with elements that increase in thickness during swelling. The concentration c_s^* is the concentration of solvent at equilibrium or maximum swelling.

concentration

$$F = \frac{\rho_s}{\rho_s - c_s M_s} \tag{2.10}$$

A method-of-lines numerical method was applied to solve the convective diffusion problem, as illustrated in Figure 2.5. We followed a similar procedure as Bisschops,[92] where diffusion of solvent caused by a gradient in solvent concentration is described on a moving grid. The initial thickness of the pure polymer film at $t = 0$ is $\delta(0)$. As solvent is penetrating from the surface into the polymer, the polymer starts to swell, causing the polymer/solvent interface to move in opposite direction. The initial polymer slab is divided in a number of layers of equal thickness, Δx_0, at $t = 0$, hence the grid points are at equal distance. During swelling, at $0 < t < t_{end}$, these grid points move with the same velocity as the polymer moves outwards (the moving grid) until solvent saturation at $t = t_{end}$. During swelling, the total film thickness, δ, increases at a velocity equal to that of the interface. At $t = 0$, diffusion of solvent starts to occur under the influence of a concentration gradient, with an equilibrium concentration c_s^* at interface, and $c_s = 0$ everywhere else, as depicted in Figure 2.5, left pane. This equilibrium concentration is calculated from the final swelling factor using Eq. 2.10. At $0 < t < t_{end}$, a solvent concentration gradient exists as schematically shown in the center pane of Figure 2.5. Note that Eq. 2.10 implies that a higher solvent concentration corresponds to a higher swelling coefficient. Therefore, the different polymer layers are expanding at different rates as long as a concentration gradient is present.

The convective diffusion equation to be solved differs from the usual form, as it has to account for simultaneous swelling. Consider a volume element at time t and solvent concentration c (we drop the subscript s for the remainder of this derivation) of volume $V = a\Delta x$, where Δx is its thickness (Δx_0 at $t = 0$) and a is its cross-sectional area. This volume element contains cV mol solvent. At time $t + \mathrm{d}t$, the solvent concentration is $c + \Delta c$, the thickness is $x + \Delta x'$, and the amount of solvent is $cV + \Delta(cV)$. By evaluating this change in amount of solvent to the difference in influx and outflux at both sides of the volume element, during Δt through surface a, we can write the finite difference equation

$$\Delta(cV) = a\left(\left(-D\frac{\mathrm{d}c}{\mathrm{d}x}\right)_{x+\Delta x} - \left(-D\frac{\mathrm{d}c}{\mathrm{d}x}\right)_x\right)\Delta t \tag{2.11}$$

With $\Delta t \to 0$ and substituting V we obtain the first order differential equation

$$\frac{\mathrm{d}(\Delta xc)}{\mathrm{d}t} = \left(-D\frac{\mathrm{d}c}{\mathrm{d}x}\right)_{x+\Delta x} - \left(-D\frac{\mathrm{d}c}{\mathrm{d}x}\right)_x \tag{2.12}$$

In absence of swelling, Δx remains constant during the diffusion process and equal to Δx_0. With an infinite number of lines, (*i.e.* letting $\Delta x_0 \to 0$), Eq. 2.12 reduces to the usual second order differential equation for convective diffusion of Eq. 2.2.

In presence of swelling, we can make use of the relation between the swelling factor and thickness

$$\Delta x = F\Delta x_0 \tag{2.13}$$

The relation between swelling factor and solvent concentration in Eq. 2.10 allows writing $c\Delta x$ as a function of c only. After differentiation, the left hand side of Eq. 2.12 then becomes

$$\Delta x_0 \left(\frac{\rho}{\rho - Mc}\right)^2 \frac{\mathrm{d}c}{\mathrm{d}t} \tag{2.14}$$

Thus, letting $\Delta x_0 \to 0$, Eq. 2.12 can be written as the second order partial differential equation

$$\frac{\mathrm{d}c(t, x)}{\mathrm{d}t} = \left(\frac{\rho}{\rho - Mc(t, x)}\right)^{-2} \frac{\mathrm{d}}{\mathrm{d}x}\left(D\frac{\mathrm{d}c(t, x)}{\mathrm{d}x}\right) \tag{2.15}$$

Note that both the diffusion coefficient D (Eq. 2.7) and the swelling factor F (Eq. 2.10) are functions of t and x. This formulation of the convective diffusion equation accounts for two effects of swelling: (1) the stretching of the polymer layers that reduces the solvent concentration gradient; (2) the dilution of penetrant in the polymer by an increase in volume. The new diffusion-swelling model is more general than Eq. 2.3 and includes both non-Fickian and Fickian diffusion. For Fickian diffusion, one would assume constant D and film thickness, which yields results identical to Eq. 2.2.

The partial differential equation in Eq. 2.15 was solved using the method-of-lines as

illustrated in Figure 2.5 with as boundary conditions

$$\begin{cases} t = 0, 0 < x < \delta & : c = 0 \\ t \geq 0, x = \delta(t) & : c = c* \\ t \geq 0, x = 0 & : \frac{dc}{dx} = 0 \end{cases}$$

It is important to note that, similar to what was assumed by Bisschops,[92] the concentration gradient is defined with respect to a moving grid. Thus, the finite difference version of Eq. 2.15 is solved for each layer of increasing thickness, and at each integration step the thickness of the slabs is updated.

Finally, we derive a relation between concentration of solvent and measured IR absorbance, as an alternative to Eq. 2.3, which assumes a constant diffusion coefficient and no sample swelling. The starting point for this derivation is Eq. 2.16, relating the absorbance of the IR band of the penetrating solvent over time, $A(t)$, to the changing concentration profile in the film, $c(t, x)$. This relation is based on the decay of the evanescent electric field strength associated with the IR beam[45]

$$A(t) = K \int_0^\delta c(t, x) e^{-2\gamma x} dx \tag{2.16}$$

Using an expression for the relative IR absorbance and concentration, allows us to use a simplified representation (Eq. 2.16) instead of the full equation used by Fieldson and Barbari.[45] In Eq. 2.16, the factor K is determined by several optical properties like the extinction coefficient and refractive indices. Using the ratio $A(t)/A_\infty$, factor K vanishes, while parameter γ is still defined as in Eq. 2.4. Due to the fast exponential decay of the evanescent wave ($e^{-2\gamma x}$), the concentration at the bottom of the film $c(t, x = 0)$ accounts for the measured absorbance $A(t)$. The relative change of solvent concentration over time can now be expressed as

$$\frac{c(t, 0)}{c(\infty, 0)} = \frac{A(t)}{A(\infty)} \tag{2.17}$$

In this model, A_t is the area of an IR band of the penetrant at time t, and A_∞ is the band area when the sample is completely saturated with penetrant (see Figure B.2).

Application of the diffusion-swelling model

Figure 2.6 shows the experimental solvent profiles and fitted curves according to the diffusion-swelling model with non-constant diffusion coefficients. In all cases, an excellent agreement was found between the experimental and fitted curves. The values obtained for D_{eq} are listed in Table 2.3. The trend in the values of solvent diffusion coefficients is similar to those determined by measurements of paint swelling on polymerised linseed oil films reported by Stolow.[93] For water, the measured diffusion coefficients are of the same order
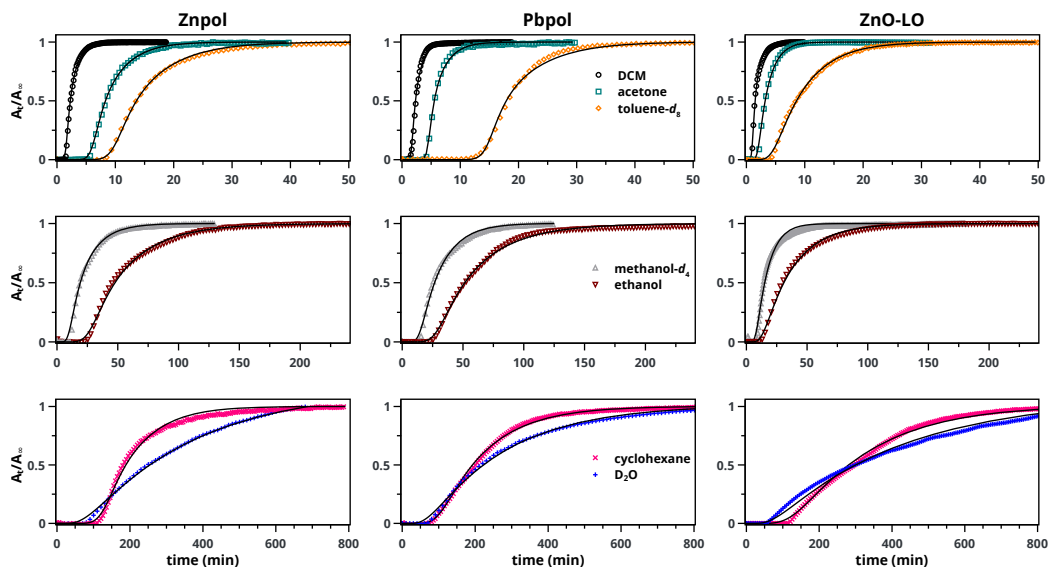
Figure 2.6 Diffusion profiles of seven solvents in Pbpol, Znpol and ZnO-LO films of 135 to 160 μm thickness and a metal ion concentration in the polymer films of roughly 420 mM. Solid black lines represent best fits of the 2-parameter diffusion-swelling model, Eq. 2.7, as employed in the convective diffusion equation, Eq. 2.15.

of magnitude as the values reported for water diffusion in pigmented alkyd paints[61] and vapor diffusion in historical samples of Prussian blue and basic lead carbonate paints[57] (ranging between $1.2 - 7.7 \times 10^{-13}$ m^2/s).

An important achievement of the diffusion-swelling model is that, unlike the (adapted) Fickian model, it gives an adequate prediction of τ_d. The values for α obtained are listed in Table B.4 and range between 0 and -19. The fact that $\alpha \leq 0$ indicates that the diffusion rate increases with decreasing polymer fraction ϕ during the transition from dry to swollen polymer. The relation between D and ϕ for solvent diffusion for **Znpol**, **Pbpol** and **ZnO-LO** is shown in Figure 2.7), highlighting the significant differences in the equilibrium swelling factor, with f_{eq} ranging between 0.05 for D$_2$O and 1.2 for DCM. The minimal values for D (D_{min}), in the dry state, are in the order of 10^{-13} m^2 s^{-1}, which is still higher than typical diffusion coefficients found for glassy polymers.[94] This finding is in agreement with the T_g values close to room temperature that we measured for dry **Znpol**, **Pbpol** and **ZnO-LO**. In general, similar diffusion coefficients (varying less than a factor of 2) were found for all three investigated model paint systems, indicating that small differences in chemical composition do not significantly affect the diffusivity. It is especially noteworthy that the introduction of 50 wt.% of pigment in **ZnO-LO** does not lead to strongly altered diffusion behaviour. This result indicates that, in intact oil paint films (*i.e.* paint films without cracks), solvent diffusion around pigment particles is relatively fast and the rate of diffusion is mostly determined by the properties of the organic polymer matrix.

Table 2.3 Values of diffusion coefficient at equilibrium swelling according to the diffusion-swelling model (D_{eq}) and those with the assumption of Fickian diffusion (D_{Fick}). Diffusion parameters have been estimated at a 95% confidence interval and were found to vary between 27–34% for D_{eq} and below 4% for D_{Fick} (Table B.3 and Table B.2). The standard deviation in the swelling factor is 0.13.

| Solvent	**Znpol**			**Pbpol**			**ZnO-LO**		
	D_{eq} 10^{-11} m²/s	D_{Fick} 10^{-11} m²/s	f_{eq}	D_{eq} 10^{-11} m²/s	D_{Fick} 10^{-11} m²/s	f_{eq}	D_{eq} 10^{-11} m²/s	D_{Fick} 10^{-11} m²/s	f_{eq}
DCM	66	14	1.2	55	14	1.1	38	16	0.66
acetone	15	4.9	0.73	23	6.1	0.89	17	7.5	0.47
toluene-d_8	8.7	2.5	0.71	9.9	3.1	0.81	3.7	2.2	0.26
methanol-d_4	5.4	1.0	0.60	2.3	0.72	0.56	2.3	1.5	0.24
ethanol	1.9	0.43	0.89	1.6	0.40	0.87	1.2	0.50	0.41
cyclohexane	0.27	0.14	0.24	0.30[a]	0.11[a]	0.45[a]	0.086	0.052	0.18
D$_2$O	0.051	0.061	0.05	0.064	0.053	0.13	0.038	0.035	0.05

[a] Measured at 40 °C
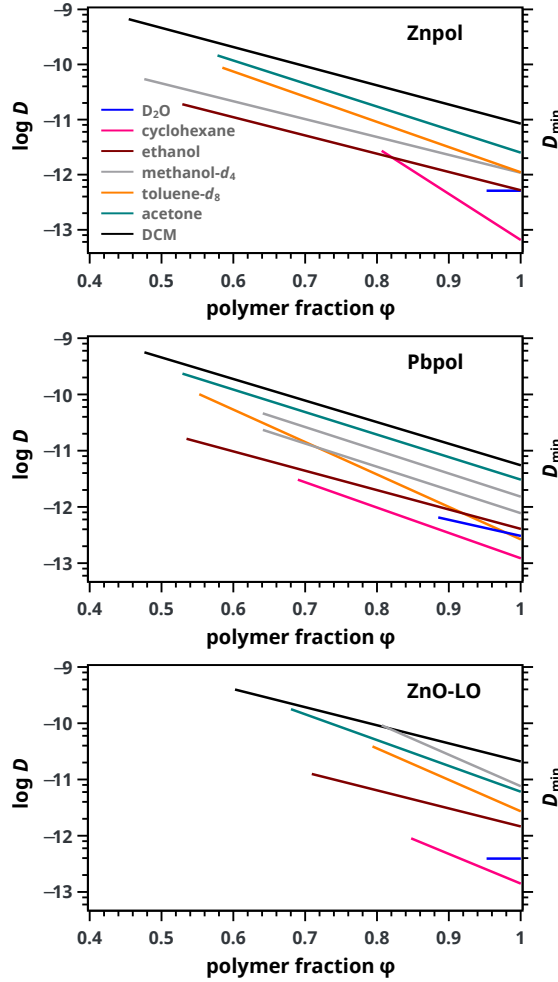
Figure 2.7 Diffusion coefficient in **Znpol**, **Pbpol** and **ZnO-LO** film versus polymer fraction ϕ, calculated using the diffusion-swelling model, Eq. 2.7, using parameters in Table B.3 and Table B.4.

Figure B.4 compares the diffusion coefficients obtained using the adapted ideal model D_{Fick} and those at equilibrium swelling obtained using the diffusion-swelling model (D_{eq}). In the adapted ideal model (Eq. 2.5), swelling effects above or inside the measurement volume after the first detection of solvent signal that slow down solvent migration are not taken into account. The diffusion-swelling model *does* incorporate this swelling, and therefore one expects $D_{\text{eq}} > D_{\text{Fick}}$. Indeed, D_{eq} is consistently larger than D_{Fick}, with the difference being largest for the most swelling solvent (DCM) and very small for the least swelling solvent (D_2O). These observations show that, even though only minor swelling occurs after solvent signal is first detected, a variable diffusion coefficient is necessary to accurately model the solvent diffusion process close to equilibrium swelling. However,

the simple adapted ideal model can still be used to calculate a reasonable approximation of the solvent diffusion coefficient. Table B.3 and Table B.4 list the obtained diffusion parameters D_{eq} and α from Eq. 2.7 values with their 95% confidence intervals for all paint models.

Having established that the swelling-diffusion model accurately describes solvent transport in oil paint systems, we can now compare diffusion parameters of the different solvents. The complexity of the solvent diffusion process is illustrated by the fact that some of the faster diffusing solvents like DCM and toluene have the highest molecular weight and that toluene and cyclohexane have very different diffusion rates despite having a similar structure. Moreover, the two slowest diffusing solvents—water and cyclohexane— are the most and least polar solvents and have the smallest and largest molecular radius in the set.

According to Amstden,[87] the parameter α of Eq. 2.6, which determines how strongly the solvent diffusion coefficient changes with polymer fraction, is related to the molecular radius of the diffusing molecule. The fitted values of α are plotted versus the molecular radius of the solvent molecules in Figure B.5. With this solvent set, we did not find a significant correlation between molecular radius and α. Since our set of solvent consists of a limited range of molecular radii and very diverse solvent properties, it is necessary to consider different solvent properties to explain the differences in diffusion behaviour. Stolow[93] correlated kinematic viscosity ν (absolute viscosity η divided by density ρ) and the diffusion coefficient. As illustrated in Figure B.6, our findings confirm this correlation, with the more slowly flowing solvents having the lowest diffusion coefficients. Water deviates from this trend with a diffusion rate that is much slower than what is expected based on its kinematic viscosity.
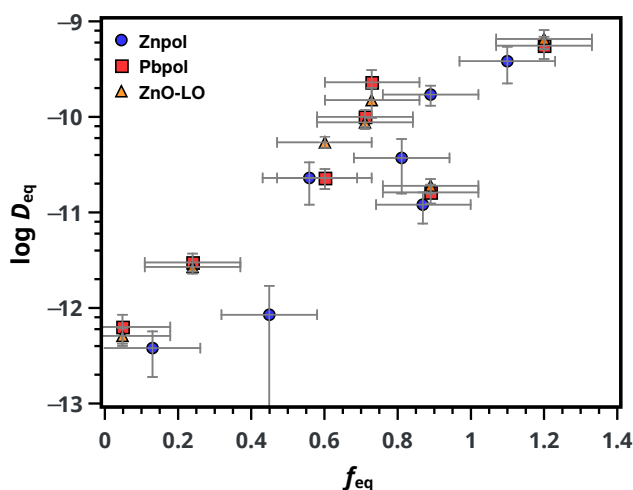
Figure 2.8 Correlation of equilibrium swelling factor, f_{eq}, with D_{eq}. Lower swelling generally leads to slower diffusion. Error bars calculated as described in Appendix A.

Historically, equilibrium swelling data has been used to quantify diffusion behavior in paints.[93] Additionally, a high degree of swelling is associated with an increased risk of pigment loss during oil paint cleaning treatments.[54] Figure 2.8 shows a logarithmic plot of D_{eq} versus f_{eq}, showing that solvents with a high swelling capacity are indeed generally diffusing faster. Alcohols exhibit relatively strong swelling compared to their moderately fast diffusion. These results confirm that swelling studies can be a useful indication of diffusion behaviour of solvents in linseed oil-based paints. However, it is important to emphasise that accurately describing diffusion phenomena in paint is not straightforward.

The experiments described in this work have practical implications for paintings restoration. Disregarding potential reactivity between the solvent and paint components, it is often desired to minimise mechanical stress and limit the volume of paint material that is affected by a solvent during cleaning. In this light, both water and aliphatic hydrocarbons like cyclohexane offer a combination of two useful properties: low swelling power and slow diffusion. As water and aliphatic hydrocarbons are at opposite ends of the polarity scale, it should be possible to remove a broad range of soiling materials from the surface of oil paintings with these two solvents. The risk of mechanical damage can be further reduced by making use of tailored gel systems for oil paint cleaning.[95,96] To this end, we would encourage the development of gel systems that can be loaded with aliphatic solvents, solvent mixtures or even microemulsions that allow precise tuning of solvent polarity. Finally, the methods described here can be extended to study paint swelling and solvent diffusion for porous paint and mixtures of solvents.

2.3 Conclusions

Paintings are exposed to organic solvents and aqueous solutions during restoration treatments, which may lead to chemical alterations within the paint layers and altered viscoelastic properties of the paint. We have characterised linseed oil based binding medium models with DMA and found viscoelastic properties similar to classical ionomers. Ionomers containing zinc show gradual broadening of tan δ with increasing metal content whereas lead ionomers show characteristic behaviour of matrix- and ion-cluster relaxation. In all cases, T_g is only weakly influenced by metal content.

Accurate concentration profiles of solvents and water in model paint samples were measured successfully using ATR-FTIR spectroscopy. Both an adapted Fickian diffusion model and a diffusion-swelling model incorporating the effect of film swelling on diffusion were used to describe the experimental data. We used the adapted Fickian model to study the solvent release of three common cleaning gels and found minimal or no solvent retention caused by the use of gels. In contrast to the adapted Fickian diffusion model, the considerable delay time observed for the relatively thick films was successfully predicted by the diffusion-swelling model. With the diffusion-swelling model, it was found that the solvent diffusion coefficients of solvents increase during paint swelling. No single

solvent parameter was sufficient to explain the measured trend in solvent swelling or diffusion rate. However, strongly swelling solvents (*e.g.* acetone) generally diffuse faster than weakly swelling solvents (*e.g.* water).

2.4 Experimental

Sample preparation Metal sorbate complexes were synthesised by dissolving 550 mg sorbic acid (Aldrich, 99+%) with 1 mL triethylamine (Sigma-Aldrich, >99%) in 20 mL demineralised water at 50 °C. The addition of 1.0 g $Zn(NO_3)_2 \cdot 6\,H_2O$ (Sigma-Aldrich p.a.) or 1.1 g $Pb(NO_3)_2$ (Sigma-Aldrich, >99 %) dissolved in 5 mL water resulted in immediate precipitation of the white product. After stirring for 20 minutes, the product was separated by vacuum filtration, washed with water followed by acetone, and dried overnight at reduced pressure. The metal sorbate salts were stored under inert atmosphere to prevent oxidation. Binding medium model systems for diffusion studies **Znpol-std.** and **Pbpol-std.** were made by grinding 250 mg zinc sorbate or an equivalent molar amount of lead sorbate with 1750 mg cold-pressed untreated linseed oil (LO, Kremer Pigmente) to a smooth paste with mortar and pestle. This concentration of metal ions is equivalent to a molar metal carboxylate to ester ratio (COOM/COOR) of 0.29, and corresponds to roughly 420 mM Zn^{2+}/Pb^{2+} in the uncured sample mixture. For DMA analysis, **Znpol** and **Pbpol** samples with constant total acid group concentration and increasing metal neutralisation were made according to Table B.1. The mixtures were applied to 50×75 mm glass slides and spread with a draw-down bar to achieve a wet thickness of 190 µm. The layers were cured overnight in an air-circulated oven at 150 °C, resulting in transparent homogeneous dark orange films with a thickness around 140 µm. Films of pure polymerised LO (**pLO**) were prepared in a similar fashion. Model paint samples for zinc (**ZnO-LO**) were made by grinding ZnO with cold-pressed untreated LO in a 1:1 (w/w) ratio to a smooth paste with mortar and pestle. The wet sample thickness was 190 µm and the samples were dried at 60 °C in air for 7 days. For all measurements, 5×5 mm squares of the films were cut and lifted off the glass support. The thickness of each sample was measured with a digital micrometer accurate to 1 µm prior to diffusion measurements.

Agar was purchased from Sigma Aldrich and Gellan Kelcogel® CG-LA (LOT NO 3H7072A) was purchased from Azelis and used as received. Gels were made by mixing 4 wt% (agar) and 3 wt% (gellan) in deionised water at 100 °C while stirring for 15 min and subsequently cast on a flat surface. Nanorestore® Max Dry was used as received from CSGI. Gels were kept in a sealed container loaded with ethanol or D_2O for at least 12 hour before use. Complete exchange of solvents inside the gels upon loading was not verified analytically. For agar and gellan, no detectable saccharide residues were found in the D_2O supernatant as analysed by ^{1}H NMR while sacharide residues were found in the ethanol supernatant. All gels were blotted with paper tissue and flushed with a flow of N_2 until dry on the surface before application.
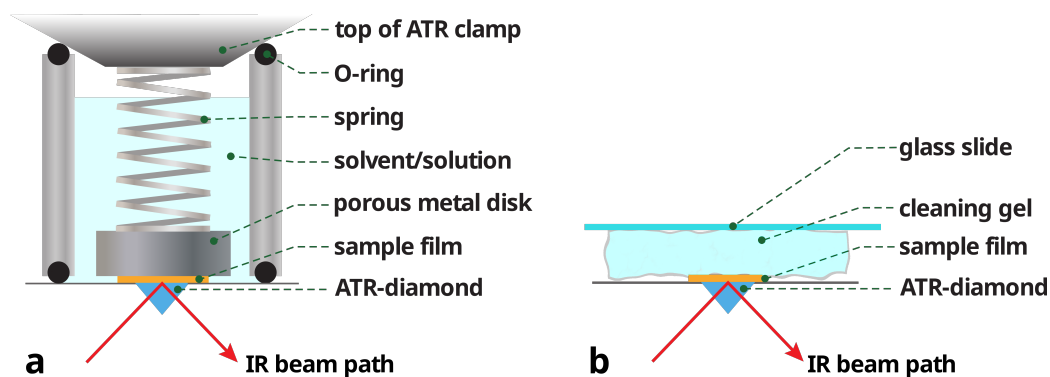
Figure 2.9 a: Illustration of the measurement cell used for time-dependent ATR-FTIR measurements of polymer films in contact with solvents. The spring provides a small pressure to keep a constant contact between the sample and the ATR-crystal as solvents swell the sample, while the porosity of the metal disk ensures unhindered diffusion of the solvent through the sample film. **b**: The setup used for the release of solvent from cleaning gels, the glass slide reduces evaporation of solvent from the gel.

Experimental setup   DMA analysis was performed on a Perkin Elmer Pyris Diamond DMA in tensile mode using a temperature range from -50 to 150 °C and a heating rate of 2 °C/min under N_2 atmosphere. For all samples, an amplitude of 10 µm, a minimum tension/compression force of 10 mN, a minimum tension/compression force gain of 1.1 mN and a force amplitude default value of 500 mN were used. The glass transition temperature (T_g) was obtained from the maximum value of tan δ. For **Pbpol**, two Gaussian functions and a baseline were fitted to determine both T_g and T_c, see Figure B.1.

ATR-FTIR spectra were measured on a Perkin-Elmer Frontier FT-IR spectrometer fitted with a Pike GladiATR module with a diamond ATR-crystal ($\varnothing$ = 3 mm). Spectra were recorded at the bottom of the sample every 10, 30 or 60 s (depending on the diffusion rate of the solvent) at 4 cm^{-1} resolution and averaged over 4 scans. In order to measure spectra of polymer samples during exposure to solvents or solutions, a custom-built stainless steel cylinder was used as illustrated in Figure 2.9. The cell volume was sealed with two solvent resistant O-rings between the top plate and the pressure clamp of the ATR module. The polymer sample was covered by a $\varnothing$ = 10 mm porous sintered metal disk, and a small but constant pressure was applied to the polymer sample by a spring placed between the pressure clamp of the ATR module and the porous disk. An inlet in the cylinder allowed for the addition of liquids to the sample chamber with a syringe. The inlet was kept sealed with parafilm during measurements to avoid solvent evaporation. In all experiments, analytical grade solvents were used. Automated spectrum collection was started as soon as solvent was injected into the measurement cell.

Data processing   Diffusion curves in polymer films were measured of cyclohexane (904 cm^{-1}), ethanol (879 cm^{-1}), acetone (529 cm^{-1}), D_2O (2510 cm^{-1}), methanol-d_4

(2485 cm^{-1}), DCM (1265 cm^{-1}), and toluene-d_8 (541 cm^{-1}). The wavenumbers in parentheses for each solvent refer to the positions of a characteristic solvent band that was sufficiently isolated for accurate band integration. The time-dependent band areas were calculated with Perkin-Elmer TimeBase software using a baseline anchored to the spectrum to either side of a band, and required no further processing before model fitting. FTIR spectra of **Znpol** at maximum solvent swelling for all solvents are shown in Figure B.2. The reproducibility of the diffusion curves was investigated by repeating the acetone diffusion experiment eight times on **Znpol** films with thicknesses varying between 124 and 159 μm. The standard deviation in the thickness measurement, caused by uneven sample surfaces, was approximately 10 %. The standard deviation in the swelling factor was determined by repeating the experiment for acetone nine times and was found to be 0.13. We have applied a method to calculate the 95% confidence intervals of the fitting parameters using a least squares procedure[97] (see Appendix 2.A). The 95% confidence interval in D_{Fick} resulting from the parameter estimation procedure was below 4%, whereas for D_{eq} the interval was between 27–34%.

Acknowledgements

2.A   Appendix A: Parameter estimation procedure

The model described in the main text is employed in the parameter estimation procedure to find the diffusion parameters, D_{eq} and α. The procedure could be performed using a direct optimisation procedure as the number of parameters to be estimated is small. The cost function, $C(\bar{D}, \alpha)$, was constructed on the basis of the values of the concentration curves from the solvent FTIR band areas, c_i, and the model predicted values, $\hat{c}_i$, on the same instants of time, t_i, over the time interval, where the concentration changes are appreciable:

$$C(\bar{D}, \alpha) = \sum_{i=1}^{N} (c_i - \hat{c}_i(\bar{D}, \alpha))^2 \tag{2.18}$$

Here, N denotes the number of time point of concentration data for each solvent/polymer sample.

Although the optimisation procedure has provided a set of parameters that allow a good description of the experimental data, yet some of the parameters could still be correlated. The estimability of such correlated parameters is problematic, they would have large error or even turn out to be completely inestimable. Therefore, we have applied a method to calculate the 95% confidence intervals of the parameters using a least squares procedure[97] based on a linearisation of the non-linear kinetic model at parameter values listed in Table B.3 and Table B.4. This method requires to calculate the sensitivity matrix X containing the partial derivatives of the observable c_i, to the parameters, D_{eq} and α:

$$X = \begin{bmatrix} \frac{1}{\sigma_c} \frac{\partial c_1}{\partial \bar{D}} & \frac{1}{\sigma_c} \frac{\partial c_1}{\partial \alpha} \\ \frac{1}{\sigma_c} \frac{\partial c_2}{\partial \bar{D}} & \frac{1}{\sigma_c} \frac{\partial c_2}{\partial \alpha} \\ \vdots & \vdots \\ \frac{1}{\sigma_c} \frac{\partial c_N}{\partial \bar{D}} & \frac{1}{\sigma_c} \frac{\partial c_N}{\partial \alpha} \end{bmatrix} \tag{2.19}$$

Here, the $\frac{1}{\sigma_c} \frac{\partial c_i}{\partial \bar{D}}$ and $\frac{1}{\sigma_c} \frac{\partial c_i}{\partial \alpha}$ denote the partial derivatives of concentration for each measurement point i to the parameters D_{eq} and α, respectively. Note that the number of rows in X equals N, the number of time point of concentration data for each solvent/polymer sample. The parameter sensitivities are numerically computed from the diffusion model and subsequently scaled with the standard deviation of concentration measurements, σ_c. The vector of standard deviations of the estimated parameters D_{eq} and α, follows as:

$$\begin{bmatrix} s_{\bar{D}} & s_{\alpha} \end{bmatrix} = \sqrt{(X^T X)^{-1}} \tag{2.20}$$

The 95% confidence interval is calculated from this standard deviation as:

$$\begin{bmatrix} s_{\bar{D}} & s_{\alpha} \end{bmatrix}_{95} = 1.96 \begin{bmatrix} s_{\bar{D}} & s_{\alpha} \end{bmatrix} \tag{2.21}$$

The value for the standard deviation of the concentration, σ_c, is obtained from 9 repeated measurements of the relative concentration curves for acetone in **ZnPol**. One value was obtained by simply constructing an average curve from the set of 9 curves and determining the standard deviation as the sum of the squared differences at each time point of the individual curves with the average curve:

$$\sigma_c = \sum_{j=1}^{9} \sqrt{\frac{1}{N} \sum_{i=1}^{N} (c_i - \bar{c}_i)^2} \tag{2.22}$$

Here, i counts the N time points ($N = 33$) at the interval, where the concentration changes appreciably, while c_i and $\bar{c}_i$ are the values of the measured and average concentrations at time points t_i. The value thus obtained was $\sigma_c = 0.087$. However, the equilibrium swelling factor and film thicknesses measured for these 9 samples are not the same, so part of the standard deviation calculated this way must be attributed to differences in swelling factor and thickness. Therefore, we decided to employ a different method to estimate σ_c, where we use the diffusion model to account for the differences in swelling factor and thickness. Using a similar cost function as Eq. 2.18 and minimising this we obtained the best fit values for D_{eq} and α for all the 9 acetone/**ZnPol** series at the measured time points: $\hat{c}_i$. Replacing $\bar{c}_i$ by $\hat{c}_i$ in Eq./ 2.20 now leads to a σ_c value corrected for swelling factor and thickness, which turned out to be $\sigma_c = 0.047$. The fact that this value is smaller is an indication indeed that part of the deviations between the 9 curves must be ascribed to differences in swelling factor and thickness. We decided that the lower estimate of σ_c is the proper value to calculate the scaled matrix X.

However, it is not sufficient to account for the error in concentration only, since the measured values of both the swelling factor and the film thickness are used, via the diffusion model, to determine the diffusion parameters, do also contain considerable error. We have determined the standard deviation of thickness, σ_δ, by measuring it repeatedly at different places on one film sample, which yielded $\sigma_\delta \approx 10^{-5}$ m. The standard deviation of the swelling factor, σ_f, as measured by the FTIR polymer band area, was obtained from the 9 acetone/**ZnPol** samples also used to estimate σ_c. Thus, σ_f turned out to be 0.13 (swelling factors are between 1 and 2.5). When determining the errors in the diffusion parameters using the sensitivity matrix, we could account for the errors in thickness and swelling factor in an elegant way by treating them as both *parameters* and *measurements* at the same time. This implies, in the first place, that we have to extend the optimisation problem with two additional parameters: thickness δ and equilibrium swelling factor f. Consequently, the starting values for these parameters of the constraint optimisation problem are set equal to their measured values, δ and f, and their constraints at $\delta \pm \sigma_\delta$ and $f \pm \sigma_f$, respectively. The second implication of treating δ and f as both parameters and measurements implies that sensitivity matrix X has two more columns and also two more rows. The extra columns denote the sensitivities of concentration to parameter

thickness, δ, and to equilibrium swelling factor, f, while the extra two rows refer to the measurements sensitivity to the parameter. As for these rows the parameters are identical to the measurements, the unscaled elements on the diagonal are just ones, as obviously $\frac{\partial \delta}{\partial \delta} = 1$ and $\frac{\partial f}{\partial f} = 1$. Since scaling by the standard deviation is required, the ultimate values of these elements become $1/\sigma_\delta$ and $1/\sigma_f$, respectively (and zeros in non-diagonal positions). Thus, we obtain an extended X matrix:

$$
X = \begin{bmatrix}
\frac{1}{\sigma_c}\frac{\partial c_1}{\partial \bar{D}} & \frac{1}{\sigma_c}\frac{\partial c_1}{\partial \alpha} & \frac{1}{\sigma_c}\frac{\partial c_1}{\partial \delta} & \frac{1}{\sigma_c}\frac{\partial c_1}{\partial f} \\
\frac{1}{\sigma_c}\frac{\partial c_2}{\partial \bar{D}} & \frac{1}{\sigma_c}\frac{\partial c_2}{\partial \alpha} & \frac{1}{\sigma_c}\frac{\partial c_2}{\partial \delta} & \frac{1}{\sigma_c}\frac{\partial c_2}{\partial f} \\
\vdots & \vdots & \vdots & \vdots \\
\frac{1}{\sigma_c}\frac{\partial c_N}{\partial \bar{D}} & \frac{1}{\sigma_c}\frac{\partial c_N}{\partial \alpha} & \frac{1}{\sigma_c}\frac{\partial c_N}{\partial \delta} & \frac{1}{\sigma_c}\frac{\partial c_N}{\partial f} \\
0 & 0 & \frac{1}{\sigma_\delta} & 0 \\
0 & 0 & 0 & \frac{1}{\sigma_f}
\end{bmatrix}
\tag{2.23}
$$

We also obtain two more standard deviations from (cf. Eq. 2.20):

$$
\begin{bmatrix} s_{\bar{D}} & s_\alpha & s_\delta & s_f \end{bmatrix} = \sqrt{(X^T X)^{-1}}
\tag{2.24}
$$

We have used the extended sensitivity matrix X to estimate the 95% confidence intervals of D_{Fick}, D_{eq} and α listed in Table B.2, Table B.3 and Table B.4. It was noted that the their values were significantly increased by mostly the error in the equilibrium swelling factor. Furthermore, treating δ and f as both parameters and measurements allowed optimisation of δ and f as well, but in only two cases this procedure yielded slightly different values for the swelling factor than the measured ones.

2.B   Appendix B: Supplementary Information
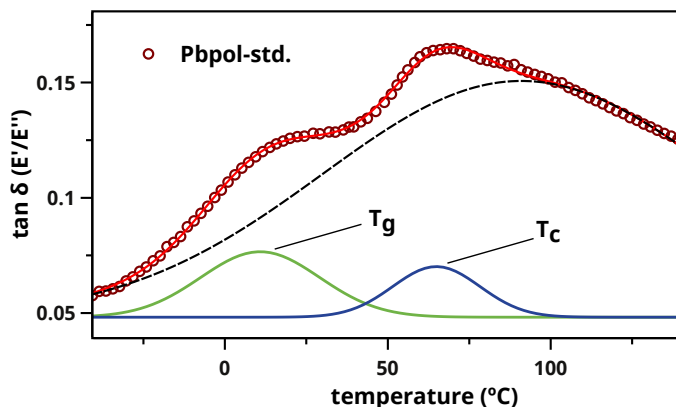
Figure B.1 Illustration of fitting procedure to obtain both T_g and T_c. The total signal intensity (red curve) is a summation of three Gaussian functions. The black dashed curve is one of the three Gaussian functions that is fitted to the experimental data, and serves as a background. The green (T_g and blue (T_c) functions correspond to the signals for the bulk glass transition and cluster glass transition, respectively.
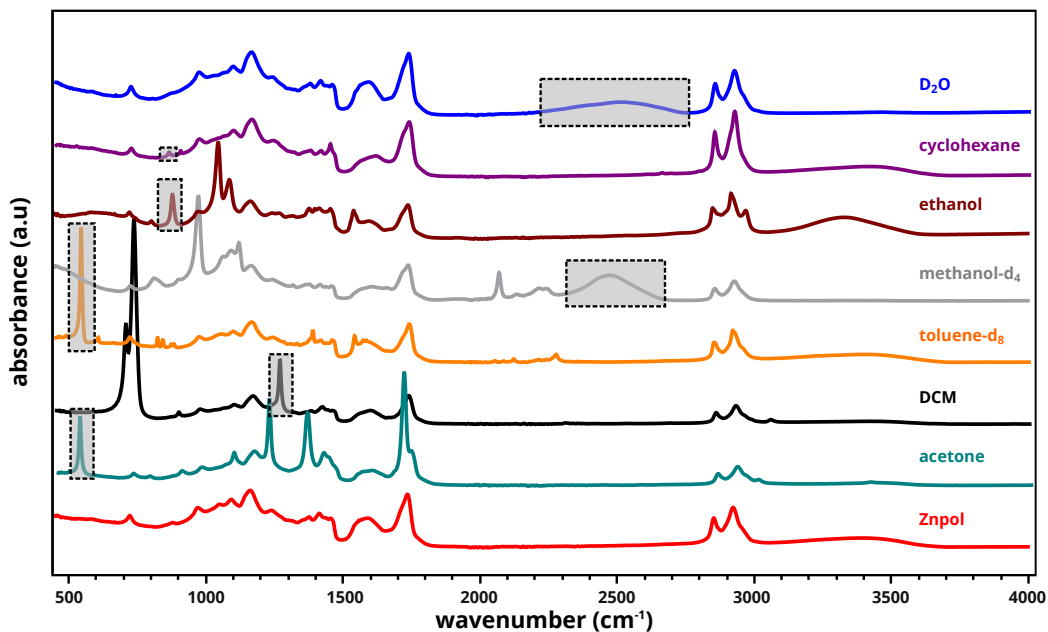
Figure B.2 FTIR spectra of solvent saturated **Znpol** ionomer samples. Dashed boxes indicate the characteristic solvent band that was integrated to measure solvent diffusion.
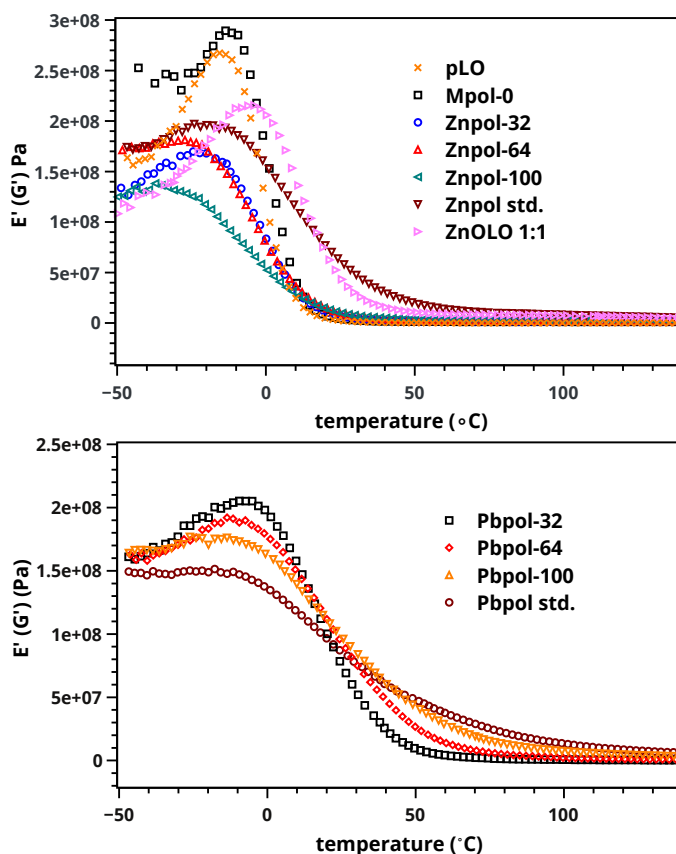
Figure B.3 Storage modulus (E') values over the temperature range -50–140 °C. Rubbery plateau region was defined at 140 °C.

Table B.1 Overview of the composition of samples for DMA measurements. LO is linseed oil, So is sorbic acid, MSo is either zinc or lead sorbate, So/LO refers to the molar ratio between sorbate molecules (either as free acid or metal complex) and linseed oil, and COOM/COOH refers to the proportion of total sorbate molecules that is bound to a metal ion (either zinc or lead).

Sample	LO (mg)	So (mg)	MSo (mg)	So/LO	COOM/COOH
pLO	400	0	0	0	0
Mpol-0	400	30	0	0.6	0
Znpol-32	400	20	12.8	0.6	0.32
Znpol-64	400	10	25.6	0.6	0.64
Znpol-100	400	0	38.4	0.6	1.00
Znpol-std.	400	0	57.1	0.2	1.00
Pbpol-32	400	20	19.2	0.6	0.32
Pbpol-64	400	10	38.3	0.6	0.64
Pbpol-100	400	0	57.5	0.6	1.00
Pbpol-std.	400	0	84.9	0.2	1.00

Table B.2 Fitted values for parameter D_{Fick} using the adapted Fickian model according to Eq. 2.3. The error in D_{Fick} values corresponds to the 95% confidence interval.

Solvent	Znpol D_{Fick} (m^2/s)	Pbpol D_{Fick} (m^2/s)	ZnO-LO D_{Fick} (m^2/s)
DCM	1.4×10^{-10} ±0.04	1.4×10^{-10} ±0.04	1.6×10^{-10} ±0.05
acetone	5.6×10^{-11} ±0.1	6.1×10^{-11} ±0.2	7.5×10^{-11} ±0.2
toluene-d_8	2.5×10^{-11} ±0.04	3.1×10^{-11} ±0.04	2.2×10^{-11} ±0.06
methanol-d_4	1.0×10^{-11} ±0.02	7.2×10^{-12} ±0.1	1.5×10^{-11} ±0.03
ethanol	4.3×10^{-12} ±0.05	4.0×10^{-12} ±0.05	5.0×10^{-12} ±0.07
cyclohexane	1.4×10^{-12} ±0.01	1.1×10^{-12} ±0.06	5.2×10^{-13} ±0.04
D$_2$O	6.1×10^{-13} ±0.01	5.3×10^{-13} ±0.04	3.5×10^{-13} ±0.03

Table B.3 Fitted values for parameter D_{eq} using the diffusion-swelling model according to Eq. 6. The error in D_{eq} values corresponds to the 95% confidence interval.

| Solvent	Znpol D_{eq} (m^2/s)	Pbpol D_{eq} (m^2/s)	ZnO-LO D_{eq} (m^2/s)
DCM	66×10^{-11} ±16	55×10^{-11} ±14	38×10^{-11} ±15
acetone	15×10^{-11} ±4	23×10^{-11} ±8	17×10^{-11} ±5
toluene-d_8	8.7×10^{-11} ±2	9.9×10^{-11} ±2	3.7×10^{-11} ±1
methanol-d_4	5.4×10^{-11} ±1	2.3×10^{-11} ±0.6	2.3×10^{-11} ±0.7
ethanol	1.9×10^{-11} ±0.4	1.6×10^{-11} ±0.4	1.2×10^{-11} ±0.3
cyclohexane	2.7×10^{-12} ±0.9	3.0×10^{-12} ±0.7	8.6×10^{-13} ±3
D$_2$O	5.1×10^{-13} ±2	6.4×10^{-13} ±2	3.8×10^{-13} ±1

Table B.4 Fitted values for parameter α using the diffusion-swelling model according to Eq. 6. The error in α values corresponds to the 95% confidence interval.

Solvent	Znpol		Pbpol		ZnO-LO	
DCM	−8.0	±0.8	−8.9	±0.79	−7.4	±1.6
acetone	−9.6	±1.5	−9.2	±1.3	−10.6	±3.0
toluene-d_8	−10.5	±1.6	−13.3	±1.8	−12.9	±7.5
methanol-d_4	−7.5	±0.6	−9.4	±1.4	−12.7	±7.7
ethanol	−7.6	±0.6	−8.0	±0.63	−7.3	±1.8
cyclohexane	−19.2	±9.1	−10.5	±1.6	−12.2	±7.3
D$_2$O	0		−6.6	±4.4	0	

Table B.5 Pure solvent properties.[98]

Solvent	D_{self} (m^2/s)	radius (Å)	density (kg/m^3)	M_W (g/mol)
DCM	3.5×10^{-9}	4.30	1330	84.9
acetone	1.3×10^{-9}	4.55	790	58.1
toluene-d_8	2.2×10^{-9}	5.38	943	100
methanol-d_4	5.9×10^{-9}	3.54	888	36.0
ethanol	2.8×10^{-9}	4.18	790	46.0
cyclohexane	3.8×10^{-9}	5.48	776	84.1
D$_2$O	5.5×10^{-9}	2.74	1100	20
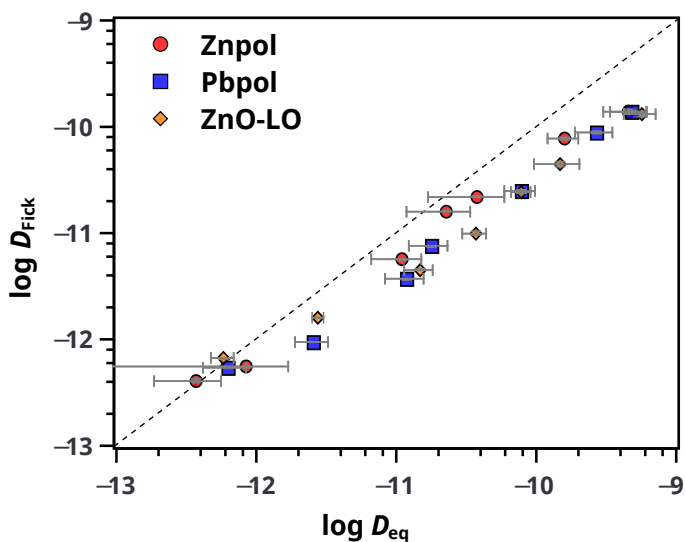
Figure B.4 Correlation between diffusion coefficient assuming Fickian diffusion (D_{Fick}) and diffusion coefficient at equilibrium swelling (D_{eq}) calculated using the diffusion-swelling model.
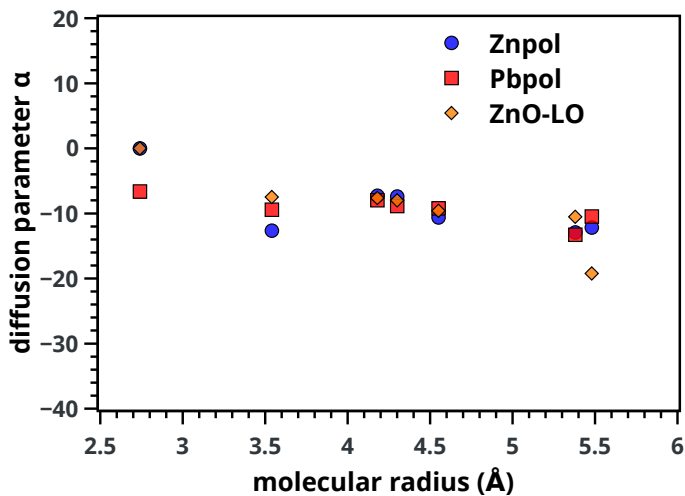
Figure B.5 Correlation between parameter α in the diffusion-swelling model with molecular radius of the solvent.
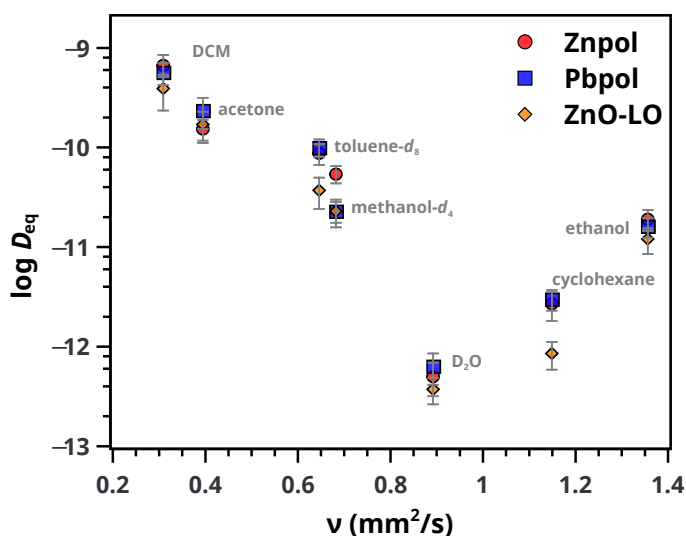
Figure B.6 The relation between the measured diffusion coefficients in Znpol for the investigated set of solvents (plotted as the natural logarithm for clarity) versus their kinematic viscosity values ν (dynamic viscosity η divided by density ρ). Kinematic viscosity values are at 298 K and taken from Ref.[98].